Near-IR Laser Absorption Measurements of Atomic Nitrogen, Oxygen, and Carbon Concentrations in Shock-Heated Air

Elijah R. Jans[1], C. M. Murzyn[2], K. A. Daniel[3], C. R. Downing[4], K. P. Lynch[5], D. J. Allen[6], and J. L. Wagner[7]
Sandia National Laboratories, Albuquerque, NM 87185

A tunable infrared laser absorption diagnostic of diatomics and atoms at 100 kHz repetition rate has been developed for measurements in shocked-heated air. The diagnostic utilizes two microelectromechanical system (MEMS) vertical cavity surface emitting lasers (VCSEL) with wavelength tuning from approximately 9,000 to 9,900 cm^{-1} and 7,300 to 7,900 cm^{-1} at 100 kHz. The diagnostic is demonstrated in the Sandia High Temperature Shock Tube (HST) for measurements in the post-reflected shock at temperatures and pressures above 8,500 K and 20 atm. Simultaneous measurements of atomic carbon (C I), nitrogen (N I), and oxygen (O I) were quantified in at these conditions. In addition, absorption measurements of the cyano radical (CN) in the $A^2\Pi_i - X^2\Sigma^+$ band system were also performed. Inferred temperature measurements agree with CEA while the number densities of the inferred atomics suggest there is nonequilibrium of the high energy electronic states of atoms.

I. Introduction

Knowledge of thermochemistry of high-temperature air experienced in hypersonic flows and re-entry velocities is crucial for understanding the radiative heating, thermal loading, and aerodynamics experienced at high flight speeds [1]. Atomic species at high shock layer temperature comprise a majority of the radiative heat flux on vehicles [2]. Ground facilities, such as shock tubes, expansion tubes, and arc jets, have been employed to generate high-temperature air for measurements of species concentrations and chemical kinetics [3]. Measurements in these facilities are challenging given the short run times, high background luminosity, and the extreme temperatures and pressures [4]. Probing such environments often times requires development of nonintrusive laser diagnostics such as emission spectroscopy [5-7], laser absorption spectroscopy (LAS) [8-11], and Coherent anti-Stokes Raman scattering (CARS) [12], which have shown success in measuring freestream parameters in shock tunnels.

[1] Post-doctoral Appointee, Engineering Sciences Center, erjans@sandia.gov, AIAA Member.
[2] Senior Member of the Technical Staff, Remoting Sensing Department.
[3] Senior Member of the Technical Staff, Aerosciences Department. AIAA Member.
[4] Principal Technologist, Diagnostics Science Department.
[5] Senior Member of Technical Staff, Aerosciences Department, AIAA Senior Member.
[6] Senior Member of the Technical Staff.
[7] Principal Member of Technical Staff, Aerosciences Department, AIAA Associate Fellow.

Sandia National Laboratories is a multi-mission laboratory managed and operated by National Technology and Engineering Solutions of Sandia, LLC., a wholly owned subsidiary of Honeywell International, Inc., for the U.S. Department of Energy's National Nuclear Security Administration under contract DE-NA0003525.

Absorption spectroscopy is a well-established diagnostic capability for characterizing gas-phase temperature and species concentrations in ground facilities [13]. The ability to infer species concentration makes absorption spectroscopy a desirable tool in the validation of chemical mechanisms and kinetic rate constants [14]. The objective of this study is to perform simultaneous absorption measurements at 100 kHz of atomic and diatomic species generated in a free-piston shock tube. Measurements of atomic carbon, nitrogen, and oxygen as well as the cyano radical are demonstrated at temperatures above 8,000 K and 20 atm in dry air.

II. Experimental Set-up

A. High Temperature Shock Tube Facility

The Sandia free-piston high-temperature shock tube (HST) is used to generate high-temperature air in the post reflected shock at elevated pressures. Details on the HST are given in more detail by Lynch et al [15] and are briefly summarized here. A reservoir section is pressurized with N_2 up to 30 atm which will launch the piston down the shock tube's driven section which contains a mixture of 10% He with 90% Ar at 11 psi. At the end of the driver section is a steel diaphragm having thickness 1.2-mm. Before the run, the driven section pulled under vacuum and filled with dry air to pressure of 2 Torr. A series of pressure transducers along the driven section measure the incident shock speed as the shock wave travels down the tube. Incident and post-reflected conditions are calculated using the NASA Chemical Equilibrium with Applications (CEA) code [16] assuming thermochemical equilibrium. Test conditions from the calculated shock and CEA results are shown in Table 1.

Table 1: Experimental Conditions

Shock Speed [m/s]	Mach	Incident Temperature (K)	Reflected Temperature (K)	Incident Pressure (bar)	Post-reflected Pressure (bar)
5333	15.5	6074	8722	1.87	24.59

B. Laser Absorption Experimental set-up

The absorption diagnostic instrument employs two commercially available microelectromechanical system tunable vertical cavity surface emitting laser (MEMS-VCSEL) (Thorlabs, SL101080 and ThorLabs SL131090) sweeping from approximately 9000-9900 cm^{-1} (1010-1110 nm) and 7400-7900 cm^{-1} (1265-1350 nm) at 100 kHz repetition rate with a 70% duty cycle. As shown in Fig. 1, each laser has a portion of its output power split between the shock tube and a wavelength reference cell. Power from the 7650cm^{-1} VCSEL is split with a 90:10 fiber (Newport: F-CPL-B12351-FCUPC) and the 9450 cm^{-1} VCSEL (1060 nm) is split with a 75:25 fiber (Thorlabs TW1064R3A1A). For wavelength reference, the 7650cm^{-1} VCSEL (1310 nm) is passed through a hydrogen fluoride (HF) gas cell (Wavelength References: HF-C(2.7)-50) with 100% HF at 50 Torr and a path length of 2.7 cm. The 9450 cm^{-1} VCSEL is passed through a C_2H_2 gas cell (Wavelength References: C2H2-12-T(9x20)-600-MgF2) at 600 Torr and a path length of 20 cm. Examples of the HF and C2H2 wavelength reference spectra are shown in Fig. 2.

Each laser is coupled to the shock tube as shown in Fig. 1. Both beams are spatially overlapped using a shortpass dichroic mirror (Thorlabs DMSP1200). The beams are angled slightly going into the shock tube to avoid etaloning on the sapphire windows. Two high-bandwidth, 5 GHz InGaAs photodiodes (Thorlabs, DET08CL) measured the transmitted laser intensity through the shock tube test section. An aspheric lens (Thorlabs, A375TM-C) with 7.50 mm focal length was mounted to each detector. In conjunction with the detector ball lens, this served to focus and compensate for beam steering. Two 4-GHz, 12-bit, 4-channel oscilloscopes (Tektronix, MSO64B) are used to record the signals at 12.5 GS/s. For each oscilloscope, channel 1 recorded the transmitted light through the shock tube. Channel 2 recorded transmitted light through a wavelength reference cell used for absolute frequency reference. Channel 3 recorded the k-clock signal form the laser, which is a relative frequency reference generated from a Mach-Zehnder Interferometer inside of the laser housing. Channel 4 was dedicated to the central wavelength trigger from the laser and used to discretize the continuous waveform in post processing. A schematic of these components is shown in Fig 1. Details regarding the calibration of oscilloscope data are provided in the following section.

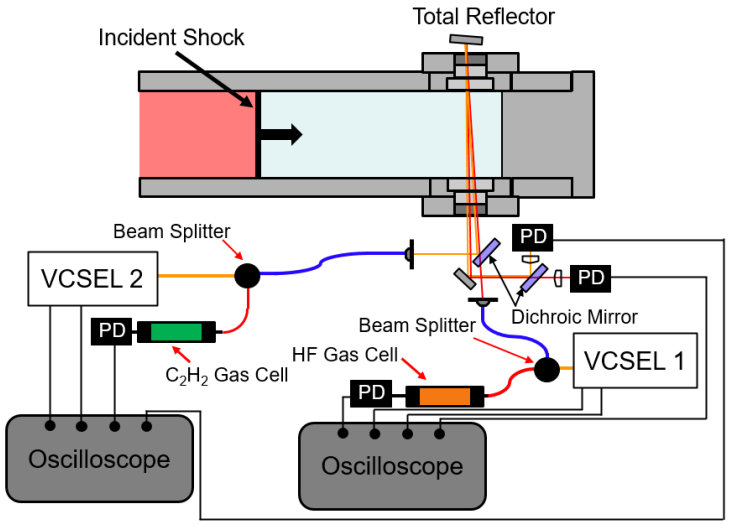

Fig. 1 Schematic of the shock tube and absorption set-up.

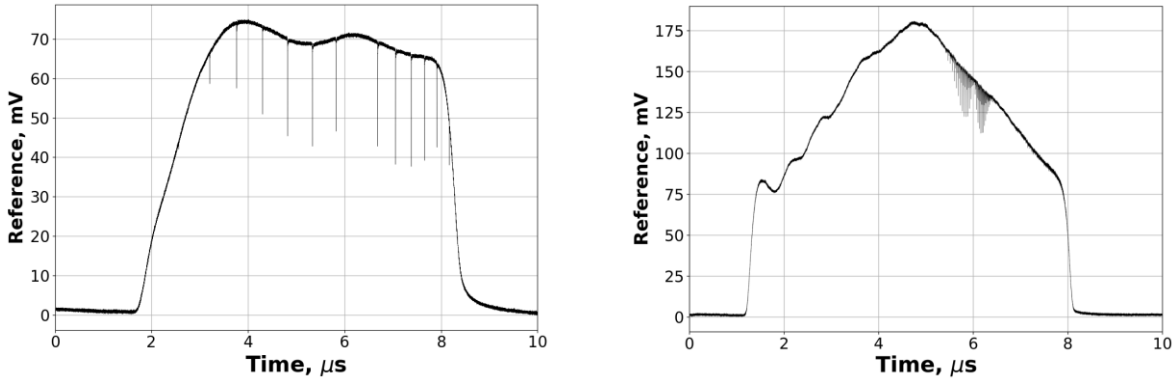

(a) (b)

Fig. 2 Wavelength reference spectrum of (a) HF for the 7650cm^{-1} VCSEL and (b) C_2H_2 for the 9450 cm^{-1} VCSEL.

III. Data Reduction and Spectral Analysis

The method for frequency-calibrating the 9450 cm^{-1} VCSEL MEMS-VCSEL is similar to that used to calibrate the 1310 nm MEMS-VCSELs in previous work [17]. In summary, the time axis from the oscilloscope is transformed into wavenumber by spline-mapping the k-clock zeros times onto a relative wavenumber grid, which is then absolutely calibrated to the reference cell. In this work, the absolute wavenumber reference was derived from a 20 cm, 600 Torr cell of acetylene $^{12}C_2H_2$. Acetylene has a vibrational mode centered around 9640 cm^{-1} with a second, weaker mode centered around 9835 cm^{-1} both of which are sufficiently absorptive for calibration.

Absorption lines used for referencing span from 9580 cm^{-1} to 9860 cm^{-1} and yield an average difference between HITRAN [18] line centers and those measured on the calibrated axis of 0.004-0.008 cm^{-1}. Additional uncertainty is introduced through the compensation of path length differences between the shock tube and acetylene optical paths. Calibration parameters yielded a sweep rate of 140 cm^{-1}/μs and 0.10349 cm^{-1} k-clock zero. Absolute frequency calibration and background reconstruction remain the predominant complexities of using MEMS-VCSELs for laser absorption spectroscopy. To fully leverage the extraordinary spectral range and resolution of these lasers requires precise wavelength calibration.

The species concentration and temperature is inferred from the experimental data using the Sandia Spectral Physics Environment for Advanced Remote Sensing (SPEARS) [19]. First, the measured intensities are converted to the spectral absorption coefficient, $\alpha(\nu)$,

$$\alpha(\nu) = \frac{1}{L_{abs}} \ln\left(\frac{I_0(\nu)}{I(\nu)}\right) \quad (1)$$

where L_{abs} is the absorption path length, $I_0(\nu)$ is the incident intensity, and $I(\nu)$ is the transmitted intensity. The incident laser intensity is taken as that during the run just before the shock wave arrives in the test section. The beam is double-passed for an absorption path length of 14.6 cm. The high temperatures and pressures in the post-reflected shock region (T > 7000 K, P > 20 atm) make determination of intensity baseline corrections difficult. The challenges include densely packed absorption lines, wide spectral lineshapes, and intensity fluctuations associated with beam steering. Thus, there is a need for effective methods for extracting signals from complex backgrounds in broadband wavelength scans. The molecular free inductive decay (m-FID) approach developed by Cole et al [20] has seen success by exploiting the temporal separability of molecular response from slowly varying background intensity using an inverse Fourier transform. Similar adaptions of the m-FID by Makowiecki et al. [21] and Goldenstein et al. [22] have seen similar success. For this work, an asymmetric least squares (ALS) algorithm [23] is applied to the inferred spectral absorption coefficient to determine the baseline. This serves to separate high and low frequency content of the spectrum. The low frequency content of the data is a summation of continuum absorption, background fit error, and power fluctuation due to flow effects (i.e., beam steering and attenuation). The ALS algorithm is also applied to each synthetic spectrum generated by SPEARS for spectral fitting.

For fitting the CN spectra, a lookup table of synthetic spectra are generated using SPEARS with the ExoMol CN database [24]. The lookup table is generated over temperatures 8000 - 10000 K with steps of 5 K and pressures from 12 - 30 atm at 0.25 atm increments. There are no reported pressure broadening coefficients for CN so the Lorentzian component of the function is calculated using the hard sphere collisional model detailed in [19]. The fitting procedure takes the sum of squared residuals for each temperature and pressure pair in the lookup table and experimental data between 9054 - 9140 cm^{-1}. This generates a two-dimensional matrix that is minimized to find the fitted temperature and pressure values. CN number densities *n* are inferred from spectral absorption coefficient and the calculated cross-section σ,

$$n = \frac{\alpha(\nu)}{\sigma(\nu)}. \quad (2)$$

For the atomic species, the inferred temperature from CN is used in the fitting process. For the fit, a Nelder-Mead optimizer was used with SPEARS to fit the Lorentzian component of the absorption lineshape. The NIST atomic database is used to determine atomic line strengths [25].

IV. Results and Discussion

Spectral absorption coefficients inferred for both lasers acquired at t = 50 μs are shown in Fig. 3(a)(b). Here t = 0 corresponds to the arrival of the reflected shock at the measurement location. The band head of the (0-0) CN A-X red system is clearly evident at ω = 9150 cm^{-1} in Fig. 3(b) and extends through the wavelength sweep of the 7650cm^{-1} VCSEL in Fig. 3(a). The experimental and best fit spectra from SPEARS of CN spectra at t = 50 μs are shown in Fig. 4(a). Excellent agreement in the overall fit can be seen between the two spectra. A heat map for the residuals is shown

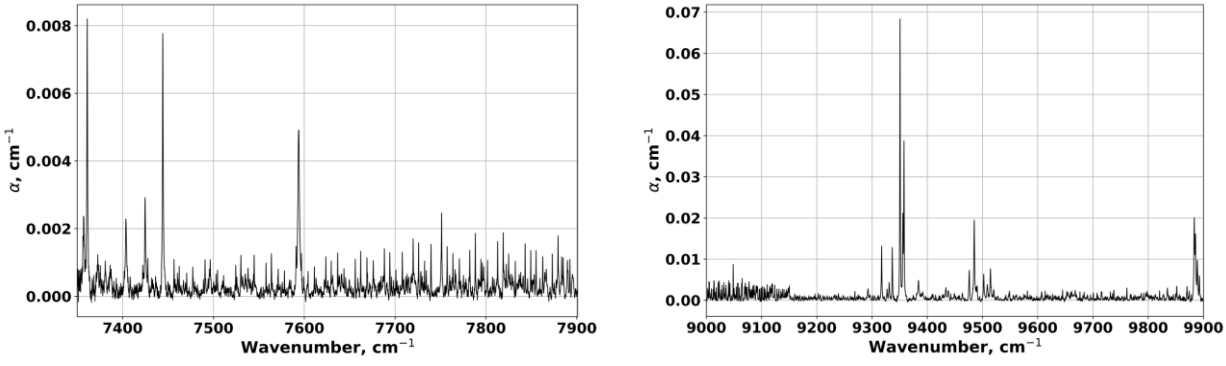

(a) (b)

Fig. 3 Inferred spectral absorption coefficient for (a) 7650cm^{-1} VCSEL and (b) 9450 cm^{-1} VCSEL.

in Fig. 4(b) from the fitting procedure with the best fit values for temperature and pressure of T = 8805 K and P =15.5 bar. The fitted pressure is less than the value in Table 1 due to the approximate nature of the hard-sphere collision model used to calculate pressure broadening in SPEARS. The time histories for the fitted temperature and number densities of CN are compared with CEA results in Fig. 5. Comparison to CEA shows a strong agreement with temperature while the inferred number densities of CN are nearly an order of magnitude higher than expected. This is possibly due to contamination inside the shock tube. Trace carbon containing species have been previously measured in the freestream of high-enthalpy hypersonic facilities [26, 27].

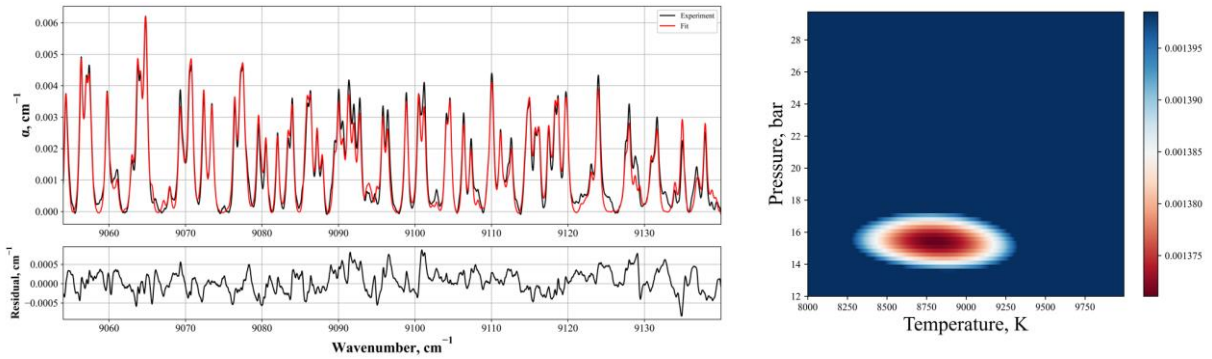

(a) (b)

Fig. 4 (a) Comparison of the experimental to best-fit synthetic spectrum of CN(A,v=0 ← X, v=0) at t = 50 μs. (b) Residual heatmap for the fitting process with fitted temperature and pressure of T = 8805 K and P = 15.5 bar.

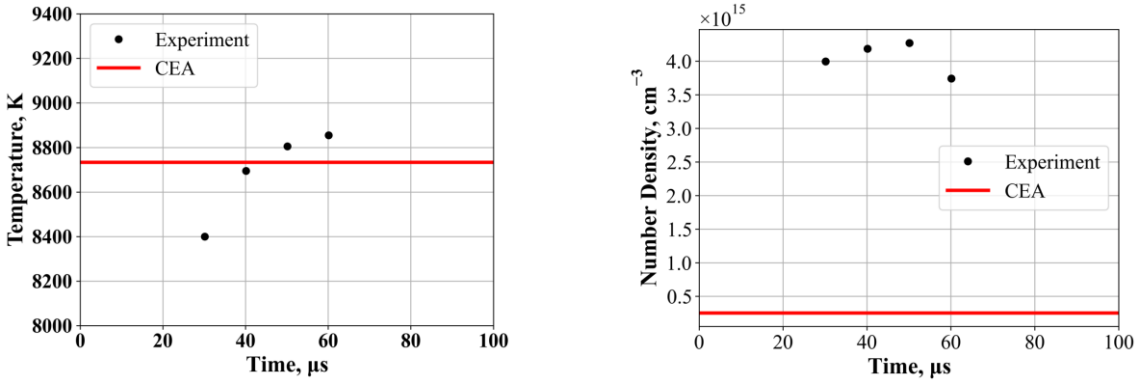

(a) (b)

Fig. 5 Time histories of the fitted (a) temperature with comparison to CEA and (b) number densities with comparison to CEA.

With time-resolved temperature measurements from CN, the absorption cross-sections can be calculated for the atomic species. Spectral fits of each atomic species are shown in Fig. 6. The resulting temporal evolution of species number densities are given in Fig. 7. Notably, the measurements suggest approximately an order of magnitude more carbon than CEA, whereas the atomic oxygen and nitrogen concentrations are an order of magnitude lower than the equilibrium calculations. These observations are possibly related to carbon contamination. An additional factor may be nonequilibrium of the high energy electronic states of these atomic species.

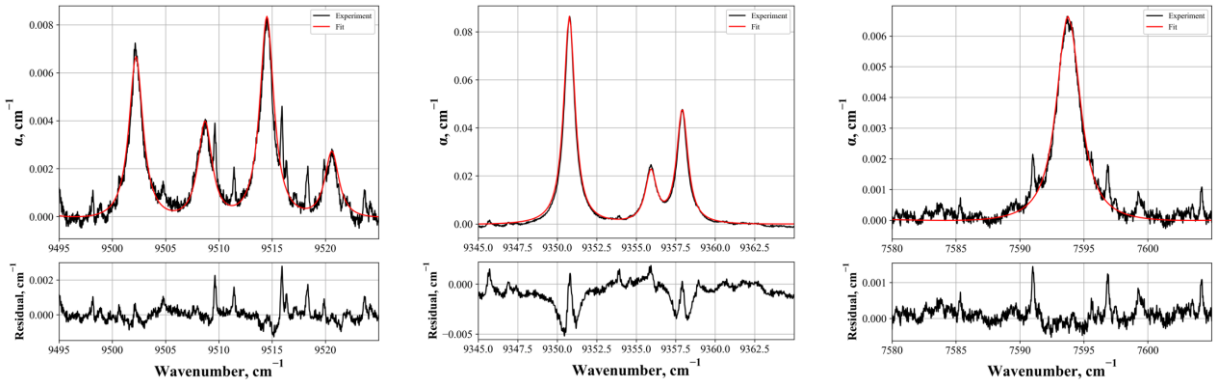

(a) (b) (c)

Fig. 6 Comparison of experimental and best-fit synthetic spectrum for (a) atomic nitrogen, (b) atomic carbon, and (c) atomic oxygen.

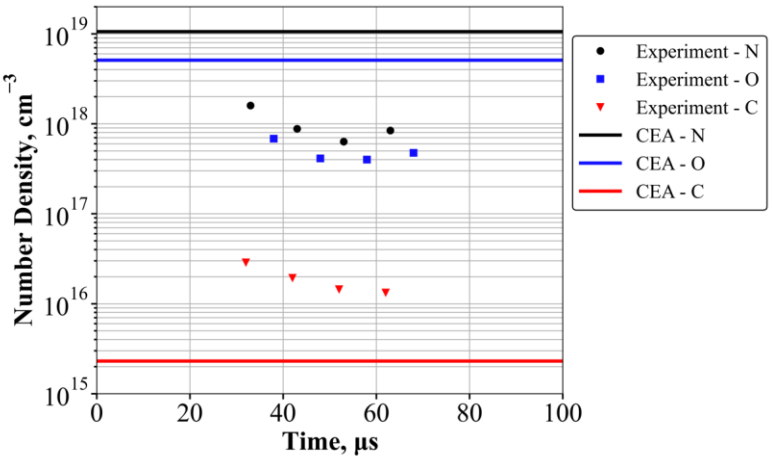

Fig. 7 Time histories of the inferred number densities of atomic nitrogen, oxygen, and carbon compared to CEA predictions at T = 8722 and P = 24.6 bar.

V. Acknowledgements

This paper describes objective technical results and analysis. Any subjective views or opinions that might be expressed in the paper do not necessarily represent the views of the U.S. Department of Energy or the United States Government. Sandia National Laboratories is a multi-mission laboratory managed and operated by National Technology and Engineering Solutions of Sandia, LLC., a wholly owned subsidiary of Honeywell International, Inc., for the U.S. Department of Energy's National Nuclear Security Administration under contract DE-NA0003525.

References

1. Johnston, C. O., Hollis, B. R., and Sutton, K. "Non-Boltzmann modeling for air shock-layer radiation at lunar-return conditions," *Journal of Spacecraft and Rockets* Vol. 45, No. 5, 2008, pp. 879-890.
2. Bose, D., McCorkle, E., Thompson, C., Bogdanoff, D., Prabhu, D., Allen, G., and Grinstead, J. "Analysis and model validation of shock layer radiation in air," *46th AIAA Aerospace Sciences Meeting and Exhibit*. 2008, p. 1246.
3. Lu, F. K. *Advanced hypersonic test facilities*: AIAA, 2002.
4. Gu, S., and Olivier, H. "Capabilities and limitations of existing hypersonic facilities," *Progress in Aerospace Sciences* Vol. 113, 2020, p. 100607.
5. Cruden, B., Martinez, R., Grinstead, J., and Olejniczak, J. "Simultaneous vacuum-ultraviolet through near-IR absolute radiation measurement with spatiotemporal resolution in an electric arc shock tube," *41st AIAA Thermophysics Conference*. 2009, p. 4240.

6. Sheikh, U. A., Morgan, R. G., and McIntyre, T. J. "Vacuum ultraviolet spectral measurements for superorbital earth entry in X2 expansion tube," *Aiaa Journal* Vol. 53, No. 12, 2015, pp. 3589-3602.
7. Tibère-Inglesse, A., and Cruden, B. A. "Analysis of nonequilibrium atomic and molecular nitrogen radiation in pure N2 shockwaves," *Journal of Quantitative Spectroscopy and Radiative Transfer* Vol. 290, 2022, p. 108302.
8. Girard, J., Finch, P. M., Schwartz, T., Yu, W., Strand, C. L., Austin, J. M., Hornung, H. G., and Hanson, R. K. "Characterization of the T5 reflected shock tunnel freestream temperature, velocity, and composition using laser absorption spectroscopy," *AIAA Propulsion and Energy 2021 Forum*. 2021, p. 3525.
9. Gilvey, J. J., Ruesch, M. D., Daniel, K. A., Downing, C. R., Lynch, K. P., Wagner, J. L., and Goldenstein, C. S. "Quantum-cascade-laser-absorption-spectroscopy diagnostic for temperature, pressure, and NO X 2 Π 1/2 at 500 kHz in shock-heated air at elevated pressures," *Applied Optics* Vol. 62, No. 6, 2023, pp. A12-A24.
10. Nations, M., Wang, S., Goldenstein, C. S., Sun, K., Davidson, D. F., Jeffries, J. B., and Hanson, R. K. "Shock-tube measurements of excited oxygen atoms using cavity-enhanced absorption spectroscopy," *Applied optics* Vol. 54, No. 29, 2015, pp. 8766-8775.
11. Streicher, J. W., Krish, A., Hanson, R. K., Hanquist, K. M., Chaudhry, R. S., and Boyd, I. D. "Shock-tube measurements of coupled vibration–dissociation time-histories and rate parameters in oxygen and argon mixtures from 5000 K to 10 000 K," *Physics of Fluids* Vol. 32, No. 7, 2020, p. 076103.
12. Kearney, S. P., Daniel, K., Wagner, J., Lynch, K. P., Downing, C. R., Lauriola, D. K., Leicht, J., and Slipchenko, M. N. "Burst-Mode Coherent Anti-Stokes Raman Scattering N2 Thermometry in the Sandia Free-Piston Shock Tube," *AIAA Scitech 2021 Forum*. 2022.
13. Hanson, R., and Jeffries, J. "Diode laser sensors for ground testing," *25th AIAA Aerodynamic Measurement Technology and Ground Testing Conference*. 2006, p. 3441.
14. von Spakovsky, M. R., and Stockwell, Z. "Theoretical Frameworks for Predicting the Chemical Kinetics of High-Temperature Flows: A Brief Review," *AIAA AVIATION 2021 FORUM*. 2021, p. 3161.
15. Lynch, K. P., and Wagner, J. L. "A free-piston driven shock tube for generating extreme aerodynamic environments," *AIAA Scitech 2019 Forum*. 2019, p. 1942.
16. McBride, B. J. *Computer program for calculation of complex chemical equilibrium compositions and applications*: NASA Lewis Research Center, 1996.
17. Murzyn, C., Allen, D., Baca, A., Ching, M., and Marinis, R. "Tunable infrared laser absorption spectroscopy of aluminum monoxide A2Πi− X2Σ+," *Journal of Quantitative Spectroscopy and Radiative Transfer* Vol. 279, 2022, p. 108029.
18. Gordon, I. E., Rothman, L. S., Hill, C., Kochanov, R. V., Tan, Y., Bernath, P. F., Birk, M., Boudon, V., Campargue, A., and Chance, K. "The HITRAN2016 molecular spectroscopic database," *Journal of Quantitative Spectroscopy and Radiative Transfer* Vol. 203, 2017, pp. 3-69.
19. Murzyn, C., Jans, E., and Clemenson, M. "Spears: A database-invariant spectral modeling api," *Journal of Quantitative Spectroscopy and Radiative Transfer* Vol. 277, 2022, p. 107958.
20. Cole, R. K., Makowiecki, A. S., Hoghooghi, N., and Rieker, G. B. "Baseline-free quantitative absorption spectroscopy based on cepstral analysis," *Optics express* Vol. 27, No. 26, 2019, pp. 37920-37939.
21. Makowiecki, A. S., Cole, R. K., Hoghooghi, N., and Rieker, G. B. "Pressure scaling of measured absorption cross-sections by modifying the molecular free induction decay signal," *Journal of Quantitative Spectroscopy and Radiative Transfer* Vol. 254, 2020, p. 107189.
22. Goldenstein, C. S., Mathews, G. C., Cole, R. K., Makowiecki, A. S., and Rieker, G. B. "Cepstral analysis for baseline-insensitive absorption spectroscopy using light sources with pronounced intensity variations," *Applied Optics* Vol. 59, No. 26, 2020, pp. 7865-7875.
23. Peng, J., Peng, S., Jiang, A., Wei, J., Li, C., and Tan, J. "Asymmetric least squares for multiple spectra baseline correction," *Analytica chimica acta* Vol. 683, No. 1, 2010, pp. 63-68.
24. Syme, A.-M., and McKemmish, L. K. "Full spectroscopic model and trihybrid experimental-perturbative-variational line list for CN," *Monthly Notices of the Royal Astronomical Society* Vol. 505, No. 3, 2021, pp. 4383-4395.
25. Ralchenko, Y., and Kramida, A. "Development of NIST atomic databases and online tools," *Atoms* Vol. 8, No. 3, 2020, p. 56.
26. Girard, J. J., Finch, P. M., Strand, C. L., Hanson, R. K., Yu, W. M., Austin, J. M., and Hornung, H. G. "Measurements of reflected shock tunnel freestream nitric oxide temperatures and partial pressure," *AIAA Journal* Vol. 59, No. 12, 2021, pp. 5266-5275.

27. Mohamed, A., Henry, D., Faléni, J., Sagnier, P., Soutadé, J., Beck, W., and Schramm, J. M. "Infrared diode Laser absorption spectroscopy measurements in the SAMA, F4 and HEG hypersonic flows," *Office national d etudes et de recherches aerospatiales onera-publications-tp*, 1999.